Mass Transfer through Vapor-Liquid Interfaces studied by Non-Stationary Molecular Dynamics Simulations

Dominik Schaefer,[1] Simon Stephan,[1, a)] Kai Langenbach,[2] Martin T. Horsch,[3] and Hans Hasse[1]

[1)] *Laboratory of Engineering Thermodynamics (LTD), TU Kaiserslautern, 67663 Kaiserslautern, Germany*

[2)] *Institute of Chemical Engineering, University of Innsbruck, 6020 Innsbruck, Austria*

[3)] *Norwegian University of Life Sciences, Faculty of Science and Technology, Department of Data Science, Drøbakveien 31, 1430 Ås, Norway*

(Dated: Wed 14th Dec, 2022)

Abstract:

Molecular dynamics (MD) simulations are highly attractive for studying the influence of interfacial effects, such as the enrichment of components, on the mass transfer through the interface. In a recent work, we have presented a steady-state MD simulation method for investigating this phenomenon and have tested it using model mixtures with and without interfacial enrichment. The present study extends this work by introducing a non-stationary MD simulation method. A rectangular simulation box that contains a mixture of two components 1 + 2 with a vapor phase in the middle and two liquid phases on both sides is used. Starting from a vapor-liquid equilibrium state, a non-stationary molar flux of component 2 is induced by inserting particles of component 2 into the center of the vapor phase in a pulse-like manner. During the isothermal relaxation process, particles of component 2 pass through the vapor phase, cross the vapor-liquid interface, and enter the liquid phase. The system thereby relaxes into a new vapor-liquid equilibrium state. During the relaxation process, spatially resolved responses for the component densities, the fluxes, and the pressure are sampled. To reduce the noise and provide measures for the uncertainty of the observables, a set of replicas of simulations is carried out. The new simulation method was applied to study mass transfer in two binary Lennard-Jones mixtures: one that exhibits a strong enrichment of the low-boiling component 2 at the vapor-liquid interface and one that shows no enrichment. Even though both mixtures have similar transport coefficients in the bulk phases, the results for the mass transfer differ significantly, indicating that the interfacial enrichment influences the mass transfer.

Keywords: vapor-liquid interface, mass transfer, binary mixture, Lennard-Jones fluid, molecular dynamics, simulation method, non-stationary, enrichment

---

[a] Electronic mail: simon.stephan@mv.uni-kl.de

I. INTRODUCTION

Mass transfer through vapor-liquid interfaces is a highly important phenomenon: it is ubiquitous in nature and applied in many technical processes, including fluid separation processes, such as absorption and distillation. While macroscopic mass transfer theories generally consider the interface as a two-dimensional object, it is well known from molecular studies that an interfacial region exists, in which the intensive properties change from the value in one bulk phase to that in the other in a continuous manner, involving steep gradients, as the interfacial region is only a few nanometers wide. Interesting phenomena occur in the interfacial region, such as the enrichment of components[1–14]. The vapor-liquid interfacial region has been studied extensively in equilibrated systems, but only little is known on the influence of mass transfer on that region and, vice versa, on the influence of that region on mass transfer. That influence is usually neglected in macroscopic mass transfer theories, but, recently, doubts on the validity of that assumption have been raised[7,10,15–21], which makes such studies all the more important.

Molecular dynamics (MD) simulations are ideally suited for investigating mass transfer through interfaces on the molecular level. Given the importance of this phenomenon, it is astonishing that, up to recently, no MD simulation methods for studying mass transfer through vapor-liquid interfaces driven by a gradient in the chemical potential have been described in the literature. We have, therefore, devised and tested two such methods. The first one is based on stationary simulation and has been published recently[22]. The second one, a non-stationary method, is described in the present work and tested using the same mixtures as in the tests of the first method. In these simulations, we address the question whether an interfacial enrichment has an influence on the mass transfer rates. The approach we take for this is straightforward: we compare results for fluxes though interfaces in a model mixture with a high interfacial enrichment with those obtained for a similar mixture that has no enrichment.

Heat transfer through vapor-liquid interfaces during evaporation and condensation has been frequently investigated in the literature using molecular simulations[23–42] and continuum models such as *density functional theory* (DFT)[31,36,40,42–46]. This inherently involves mass transfer, but the focus of the studies is different from ours; furthermore, in most of these studies, only pure components were considered. Stationary mass transfer through pores, membranes, crystals [47–53], and homogeneous fluid phases [54–56] induced by a gradient of the chemical potential has been subject of several studies. However, these studies do not involve vapor-liquid interfaces. In these studies, the gradient was usually created using the so-called dual-control volume (DCV) method[49,52,57–59]. In the recent work of our group[22], that was already mentioned above, we have adapted the DCV method to induce a stationary flux of a component through the vapor-liquid interface of a binary mixture. The simulation method for quasi-stationary mass transfer through a vapor-liquid interface driven by a gradient in the chemical potential was adapted in a recent study by *Rauscher et al.*[60] with the extension of a temperature gradient to investigate mass and heat transfer at interfaces of similar mixtures of simple fluids.

Non-stationary mass transfer close to and in the interfacial region has been investigated by several studies using different techniques: *Baidakov et al.*[61,62] have investigated the dynamic formation of vapor-liquid interfaces in pure substances and binary mixtures and the evolution of interfacial properties in the process. In their studies, first a system containing a coexisting vapor and liquid phase was equilibrated. After the equilibration, all particles in the interface layer were instantaneously removed and the non-stationary relaxation process and formation of a new vapor-liquid interface was observed. *Bucior et al.*[63] have studied evaporation of a pure liquid in a slit pore into a spontaneously created vacuum by moving the pore walls. *Nagl et al.*[15] studied the non-stationary mass transfer through liquid-liquid interfaces of different real fluid mixtures using a combination of experiments and theoretical calculations. *Braga et al.* investigated self-diffusion at liquid-liquid interfaces [64] and the free energy barrier at vapor-liquid interfaces[65] by moving a probe particle through the respective interface. *Garrett et al.*[66] observed the trajectories of single particles moving in the vicinity of a vapor-liquid interface in aqueous systems under equilibrium conditions and categorized four different behaviors of these particle: adsorption, absorption, desorption, and reflection.

In the present work, we describe a new simulation method for studying a non-stationary mass transfer through vapor-liquid interfaces of mixtures: First, the system containing only particles of one component is equilibrated. The initial equilibrium state consists of a liquid phase slab surrounded by a vapor bulk phase, which coexist in a rectangular simulation box with periodic boundary conditions. After the first equilibration, particles of a second component are inserted in the middle of the vapor phase during a short period of time, i.e. in a pulse-like manner. This perturbation induces a non-stationary, one dimensional flux of the inserted particles towards the two vapor-liquid interfaces and through them into the liquid phase on both sides of the vapor phase. The process is basically symmetric with regard to these interfaces. The relaxation process caused by the perturbation is then studied, focusing on the processes in the vicinity of the interfaces. Simulations are run until a second, final equilibrium state is reached.

A major problem of non-stationary molecular dynamics simulations is to distinguish an actual physical process from random noise and to provide a measure of uncertainty. Therefore, our simulation study was performed using *sets of replicas*, i.e. the simulation was repeated several times using different initial velocity distributions. The simulation box and start system size, temperature, and the insertion procedure were the same for all simulations in a set of replicas. The results obtained from a set of replicas were averaged, resulting in a reduction of the noise of the signal; furthermore, a measure for the statistical uncertainties of the observables was obtained. This replica strategy based on varying starting conditions is a well-established method in non-stationary molecular dynamics simulations[65,67–70].

The new simulation method was applied to investigate non-stationary mass transfer in two binary Lennard-Jones mixtures with distinctively different phase behavior. Both mixtures (referred to as mixture A and B in the following) have been studied extensively by our group regarding thermodynamic [10,16,71–73] and transport properties[22]. Equilibrium molecular dynamics simulations and density gradient theory consistently yield a strong enrichment of the low-boiling component at the interface for mixture A, while no such enrichment is found in mixture B[10,16,22,71–73]. The same mixtures have been used in the quasi-stationary approach of our recent study[22].

An enrichment of low-boiling components at equilibrium conditions has been reported for many mixtures of real fluids and model fluids[1–13]; see Ref.[74] for a recent review. It has been discussed in various studies[7,10,15–21] that the enrichment might have an influence on the diffusive mass transfer through the interface (which would be in line with Fick's law), but to date there is no proof of this hypothesis. No experimental studies of this are available, nor are they to be expected in the foreseeable future, since the enrichment occurs in the interfacial region, which is only a few nanometers wide and fluctuates, which hinders the acquisition of meaningful experimental data. Hence, we have to rely on simulation methods for corresponding studies.

This paper is structured as follows: First, the simulation method is introduced. Then, the studied test mixtures are described. Next, the simulation results from one temperature are discussed in detail comparing the results from both mixtures. Finally, results obtained for several temperatures are compared, which provides insights into the temperature dependency of the relaxation process.

II. SIMULATION METHOD

A. Overview

The basic concept of the simulation method is illustrated in Figure 1. The simulation box has a rectangular shape and periodic boundary conditions in all directions. At the start, the simulation box only contains particles of component 1. The conditions are chosen so that the box contains two phases: a vapor phase in the middle of the simulation box surrounded by a liquid phase. During the entire simulation run, the number of particles of component 1, the temperature, and the volume of the simulation box are kept constant. After establishing the vapor-liquid equilibrium state of the pure component 1 system, it is perturbed by the insertion of particles of component 2, which are inserted in the control volume (CV) in the middle of the vapor phase, cf. Figure 1. The response of the system to that perturbation is evaluated until the system relaxes into a second vapor-liquid equilibrium state. Except for statistical fluctuations, the process is symmetric with respect to a plane in the middle of the simulation box.

Hence, a simulation run consists of the following five phases:

1. Initial equilibration phase (*IniEq*)
2. Sampling phase of the first vapor-liquid equilibrium state (*Eq1*)
3. Insertion phase (*In*)
4. Relaxation phase (*Relax*)
5. Sampling phase of the second vapor-liquid equilibrium state (*Eq2*)

The abbreviations in the brackets are used in the following for brevity.

The first two simulation phases *IniEq* and *Eq1* are carried out in the NVT ensemble. Subsequently, in the *In* phase, particles of component 2 are inserted in the center of the vapor bulk domain, cf. Figure 1. The insertion of particles of component 2 inside the control volume is performed using a Monte Carlo algorithm[54,57,58], that adjusts the number of particles of the component 2 based on a prescribed chemical potential of that component $\mu_{2,\mathrm{CV}}$. Since the chemical potential is only controlled in a sub-volume of the entire simulation box (cf. Figure 1), the *In* phase can be considered a quasi-μVT ensemble.

With the beginning of the particle insertion, a one dimensional, non-stationary molar flux j_2 of particles of component 2 is established. The molar flux is positive on the right of the control volume and negative on the left of the control volume due to the symmetry of the simulation box setup, cf. Figure 1. During the *Relax* phase the system re-equilibrates to the second equilibrium state point, which is sampled over the course of the *Eq2* phase. The *Relax* and the *Eq2* phase are again carried out in the NVT ensemble.

B. Definition of Observables and Data Processing

The simulation box is discretized in z-direction into 1,200 equally sized bins. Since a planar interface is studied, no bin-discretization in x- and y-direction is applied, i.e. the simulation scenario is quasi-one-dimensional. Observables $\chi(\tau, z)$ are sampled in these bins as a function of the z-direction and time τ every 10,000 simulation steps. The studied observables are the pressure tensor p, the density ρ_i, and the mole composition x_i of a component i. The rate of change of the density $\partial\rho_i/\partial\tau(\tau, z)$, which is needed for the determination of the molar flux j_i, is determined for each bin separately by numerical differentiation with respect to the time τ.

The position of the liquid film and its interfaces is not fixed in the simulation box and can therefore freely move during the simulation run (it fluctuates and changes slightly due to the absorption of component 2). The positions $z_{50} = z(\rho_{50})$ of the two interfaces as well as the positions $z_{10} = z(\rho_{10})$ and $z_{90} = z(\rho_{90})$ were determined by the z-position, where the local total density corresponds to 10 %, 50 %, and 90 % of the bulk density difference, i.e.

$$\begin{aligned} \rho_{10} &= \rho^{''} + 0.1(\rho^{'} - \rho^{''}) \ , \\ \rho_{50} &= \rho^{''} + 0.5(\rho^{'} - \rho^{''}) \ , \\ \rho_{90} &= \rho^{''} + 0.9(\rho^{'} - \rho^{''}) \ , \end{aligned} \tag{1}$$

where $\rho^{''}$ indicates the total vapor bulk phase density and $\rho^{'}$ the total liquid bulk phase density. Details on the procedure to determine ρ'' and ρ' are given in the Supporting Information.

In the following, the data processing procedure is described for the right interface only (cf. Figure 1). The interface on the left is evaluated applying an equivalent procedure and results for both interfaces are averaged. The molar flux j_2 of the inserted particles of component 2 is determined by solving the molar balance of each bin per time step. Particles of component 2 may enter or leave a bin over its two boundaries, thus there are two molar flux j_2 per bin. The molar flux j_2 is always the net molar flux here. A positive flux is directed in positive z-direction and, accordingly, a negative flux is directed in negative z-direction. In the following, the index $n = 1...N$ denotes bins and the flux at the left bin boundary has the index n while the flux at the right bin boundary has the index $n{+}1$. The molar balance of a bin n for particles of component 2 at a time step τ can therefore be written as

$$\frac{\partial \rho_2}{\partial \tau}(\tau, n) = -\frac{j_2(\tau, n{+}1) - j_2(\tau, n)}{\Delta z_{\mathrm{bin}}} \ , \tag{2}$$

where Δz_{bin} is the size of the bin and j_2 is the molar flux of component 2. To obtain $N{+}1$ unknown molar fluxes of N bins, N molar balances have to be solved (cf. Eq. (2)) with the help of a boundary condition. In this work, the symmetry boundary condition applies, according to which the net flux in the middle of the liquid slab is zero (cf. Figure 1). The position of the middle of the liquid slab is determined as the midpoint between the positions z_{50} of the two interfaces in each time-step and, hence, may fluctuate during the simulation. The gradient and molar balances are determined in a fixed reference frame in each time step, only the position, where the symmetry boundary condition is applied, moves according to the position of the middle of the liquid slab. This is done for each simulation in a set of replicas independently and results are averaged at the position of the middle of the liquid slab. The density, composition, and pressure tensor sampled in a bin n at the same time τ are averaged over all simulations in a set of replicas. This procedure significantly reduces noise and enables the estimation of the statistical uncertainty for each sampled observable χ.

The start and end time of the *In* phase are the same for all simulations. The number of inserted particles in a set of replicas varies due to the probabilistic nature of the Monte Carlo algorithm. The number for $\mu_{2,\mathrm{CV}}$ was chosen so that the mean number of inserted particles in set of replicas was 1,200 particles. The distribution of the number of inserted particles in a set of replicas is quite narrow (standard deviation about 1.5 %). Preliminary tests showed that this yields a satisfactory signal-to-noise ratio for the observables of interest such as density, pressure, and molar flux during the simulation run. Details are given in the Supporting Information.

The behavior of the system in the vapor phase and the liquid phase in the vicinity of the vapor-liquid interface is of particular interest. The relaxation process is sampled in two measurement volumes (MV) close to the interface: one in the bulk vapor phase and one in the bulk liquid phase (here labeled with $\mathrm{MV}_{\mathrm{vap}}$ and $\mathrm{MV}_{\mathrm{liq}}$, respectively). The position of these measurement volumes is defined with respect to the interface position, as illustrated in Figure 2. Figure 3 illustrates the simulation procedure, the responses to the perturbation in vapor and liquid phase determined from a set of replicas as well as the five phases of the non-stationary simulation method.

III. APPLICATION OF THE SIMULATION METHOD

A. Binary Lennard-Jones Mixtures

The Lennard-Jones (LJ) fluid is computationally inexpensive, but is able to reliably describe properties of simple fluids[75,76], which makes it well-suited for testing new methods in molecular simulations. In the present work, the so-called truncated and shifted Lennard-Jones potential (LJTS) was used, with a cut off radius of $r_c = 2.5\,\sigma$:

$$u_{\mathrm{LJ}}(r) = 4\varepsilon \left[\left(\frac{\sigma}{r}\right)^{12} - \left(\frac{\sigma}{r}\right)^{6} \right] \quad \text{and} \tag{3}$$

$$u_{\mathrm{LJTS}}(r) = \begin{cases} u_{\mathrm{LJ}}(r) - u_{\mathrm{LJ}}(r_{\mathrm{c}}) & r \leq 2.5\,\sigma \\ 0 & r > 2.5\,\sigma \end{cases} . \tag{4}$$

Here, $u_{\mathrm{LJ}}(r)$ is the potential energy of the LJ potential between the particles[77], which depends on their distance r. For the cross-interactions of unlike particles in the mixtures, the modified Lorentz-Berthelot combination rules were applied[78,79]

$$\sigma_{ij} = \frac{\sigma_i + \sigma_j}{2} \tag{5}$$

$$\varepsilon_{ij} = \xi_{ij}\sqrt{\varepsilon_i \varepsilon_j} \tag{6}$$

in which an additional binary parameter ξ_{ij} is introduced (cf. Eq. (6)), which has an important influence on the phase behavior of binary mixtures[71].

The simulation method proposed in this work is applied to two different binary LJTS mixtures. For both mixtures, the size parameter σ_i and mass m_i of component 1 and 2 are equal and set to unity. Also the energy parameter of component 1 ε_1 is set to unity while ε_2 of the components 2 is different for the two mixtures. The same holds for ξ_{12}. The parameters of the two studied test mixtures are given as:

- Mixture A: $\varepsilon_2/\varepsilon_1 = 0.6$ and $\xi_{12} = 0.85$
- Mixture B: $\varepsilon_2/\varepsilon_1 = 0.9$ and $\xi_{12} = 1.00$

The phase behavior and interfacial properties of these two LJTS mixtures have been investigated systematically in previous works of our group[10,16,71–73]. Their thermophysical properties were therein found to be well described by the PeTS equation of state[10,80]. The resulting phase equilibria of the mixtures A and B at the temperatures that were studied in the present work are shown in Figure 4. Mixture A has an asymmetric, wide-boiling phase behavior, whereas mixture B has essential an ideal phase behavior in the sense of Raoult's law. Mixture A also exhibits a vapor-liquid-liquid equilibrium (VLLE) at the lowest studied temperature. Even though both mixtures have distinctively different phase behaviors, they have similar diffusivity (the product of density and the mutual diffusion coefficient) in the vapor and liquid phases[22]. In mixture A, the low-boiling component exhibits a large enrichment at the vapor-liquid interface in thermodynamic equilibrium[10,72], i.e. the number density $\rho_2(z)$ shows a distinct maximum at the interface. In mixture B, no such enrichment is present.[10,72]. The two mixtures also differ in other interfacial properties such as the surface tension, the interfacial thickness, and the relative adsorption of the low-boiling component at the interface; for details see[72].

In the following, all physical properties are reduced using the LJ potential parameters of the high-boiling component 1 (σ_1, ε_1, m_1) (which are equal for both considered mixtures) and the Boltzmann constant k_B[77,81].

B. Simulation Details

For the simulations carried out in this work, the simulation box had a rectangular shape with a length l_z in z-direction of $l_z = 150\,\sigma$ and a quadratic cross section in x- and y-direction with a side length of $l_y = l_x = 27.85\,\sigma$. The temperature was controlled by the velocity scaling thermostat[77]. The control volume had a length in z-direction of $\Delta z_{\mathrm{CV}} = 10\,\sigma$ and the same quadratic cross section in x- and y-direction as the simulation box. The time step was $\Delta\tau = 0.001\,\sigma(m/\varepsilon)^{1/2}$. The total run time was $\Delta\tau_{\mathrm{Sim}} = 4,500\,\sigma(m/\varepsilon)^{1/2}$ for all simulations. The duration of the five simulation phases was $\Delta\tau_{\mathrm{IniEq}} = \Delta\tau_{\mathrm{Eq1}} = 500\,\sigma(m/\varepsilon)^{1/2}$, $\Delta\tau_{\mathrm{In}} = 100\,\sigma(m/\varepsilon)^{1/2}$, $\Delta\tau_{\mathrm{Relax}} = 2,900\,\sigma(m/\varepsilon)^{1/2}$, and $\Delta\tau_{\mathrm{Eq2}} = 500\,\sigma(m/\varepsilon)^{1/2}$. During the *In* phase 50 MC insertion/removal trials were performed every 40 MD steps within the control volume to prescribe the chemical potential. The vast majority of accepted MC trials were insertion moves, as expected.

Each set of replicas contained 100 simulations. The initial configuration a set of replicas contained 16,000 particles of component 1. Observables χ of bins at the same position n and time τ of each simulation in a set of replicas were arithmetically averaged and the uncertainty of each observable χ of a set of replicas was computed with the single standard deviation. Observables χ sampled in each bin were averaged each $\Delta\tau = 10\,\sigma(m/\varepsilon)^{1/2}$ time interval. Each bin had a length in z-direction of $\Delta z_{\mathrm{bin}} = 0.125\,\sigma$ and the same quadratic cross section in x- and y-direction as the simulation box. Overall, the simulation box was discretized in z-direction into 1,200 bins. The rectangular measurement volumes $\mathrm{MV}_{\mathrm{liq}}$ and $\mathrm{MV}_{\mathrm{vap}}$ had a length in z-direction of $\Delta z_{\mathrm{MV}} = 1\,\sigma$ and had a quadratic cross section with the same side length as the simulation box in x- and y-direction. The two measurement volumes were positioned at a distance of $\Delta z_{\mathrm{off}} = 7\,\sigma$ from the characteristic interface positions z_{10} and z_{90} (cf. Eq. (1) and Figure 2), respectively. The molar fluxes in and out of the measurement volumes were sampled at the boundaries of the measurement volume in positive and negative z-direction. In the further course of this work for each measurement volume only the molar flux at the boundary closest to the interface is shown and discussed. The simulations in this work were carried out using the open source molecular dynamics code *ls*1[82].

IV. RESULTS AND DISCUSSION

In this work, for each of the two studied mixtures, the same four temperatures were investigated, which yields 8 sets of replicas, each containing 100 simulations. First, in section IV A, the results for both mixtures for the temperature $T = 0.715\,\varepsilon k_{\mathrm{B}}^{-1}$ are presented and discussed in detail. An overview of the results for other temperatures are discussed in section IV B, details and the corresponding numerical data are presented in the Supporting

Information. Table I summarizes the main simulation settings and some key simulation results for all studied sets of replicas: the temperature T and the chemical potential $\mu_{2,\mathrm{CV}}$ prescribed in the control volume as input parameters as well as the mean number of particles N_2 inserted in the *In* phase, the vapor pressure of *Eq1* and *Eq2* as well as the vapor and liquid phase density of component 2 in the *Eq2* phase.

A. Results for the Temperature $0.715\,\varepsilon k_\mathrm{B}^{-1}$

1. Response in the Liquid and the Vapor Phase

Figure 5 presents the results obtained in the replica studies carried out for $T = 0.715\,\varepsilon k_\mathrm{B}^{-1}$ with the two mixtures A and B. Besides the mean value obtained from the averaging of the replica results, also the standard deviation is depicted. Results from the sample volumes on the vapor side (MV_vap) and the liquid side (MV_liq) are shown for three observables: the density of component 2, the flux of component 2, and the pressure.

Let us first discuss the uncertainty of the results. For both mixtures and both measurement volumes, the noise of the results for the density is of the order of 10 %, cf. Figure 5, which is low considering the difficulty of the spatially and temporally resolved measurement of a small quantity. Results of a similar quality were obtained for the pressure in the measurement volume in the vapor phase. In contrast, the uncertainty of the results for the pressure in the measurement volume in the liquid phase is high, which is not astonishing regarding the extreme sensitivity of this property[83,84]. As the flux of component 2 was not measured directly but derived from the results for the density, no standard deviation is reported. Fast changes in the pressure and the density of component 2, that occur during and shortly after the *In* phase, would not be recognizable as physically meaningful without the averaging procedure of the set of replicas.

In the initial equilibrium state *Eq1*, which is the same for both mixtures, only component 1 is present. The component 2, which is different for mixture A and mixture B, is only added in the insertion phase *In*. Shortly after the beginning of the insertion, the density of component 2 and the pressure in the measurement volume MV_vap increase steeply. There is a short time-delay until the first component 2 particles reach the measurement volume MV_vap. As a consequence, also the molar flux of component 2 j_2 in the measurement volume

$\mathrm{MV_{vap}}$ rises steeply in both simulations. All observables shown in Figure 5 peak shortly after the insertion phase has ended.

The following relaxation to the second equilibrium state *Eq2* is different for the mixture A and the mixture B, which is partially a consequence of the differences in the equilibrium state *Eq2* for the two mixtures. The solubility of the light-boiling component 2 in the liquid component 1 is significantly lower for mixture A than for mixture B[71,73]. This is caused by the lower value of ε_2 (causing a higher volatility of component 2), as well as by the lower value of ξ_{12} (less favorable mixed dispersive interactions) in mixture A. As a consequence, the final values of the density ρ_2 in the liquid phase are much lower for mixture A than for mixture B (Figure 5 (b)), while it is vice-versa for the gas phase (Figure 5 (a)). The higher amount of component 2 in the gas phase also causes the higher pressure observed for mixture A in the final equilibrium state *Eq2* (Figure 5 (e) and (f)). As expected, that pressure is the same in both measurement volumes. The lower solubility of component 2 in mixture A also explains why the integral under the molar flux of component 2 in the measurement volume in the liquid phase $\mathrm{MV_{liq}}$ shown in Figure 5 (d), is much smaller than the corresponding integral for mixture B. The time constant of the relaxation process is of the same order of magnitude for both studied mixtures. The relaxation for mixture B is slightly slower, which is attributed to the fact, that more of component 2 has to be transferred into the liquid phase, before the new equilibrium state is reached. The time-dependent changes in the pressure are basically a consequence of the mass transfer, as the mechanical equilibrium is established very fast.

As explained above, there is a maximum in all observables shown in Figure 5 in the vapor phase measurement volume $\mathrm{MV_{vap}}$ that is reached shortly after the end of the insertion phase *In* (Figure 5 (a),(c),(e)). After passing through that maximum, for the mixture B, all observables simply decay to their values in the second equilibrium state *Eq2*. At about $\tau = 1,200\,\sigma(m/\varepsilon)^{1/2}$, a slight change of the way the decay takes places is noticeable, which is best visible as a small hump in the signal for j_2 (Figure 5 (c)).

The corresponding findings for mixture A are completely unexpected: after having passed the maximum, the density ρ_2 measured in $\mathrm{MV_{vap}}$ for mixture A first decreases and then rises again to approach its value in the equilibrium state *Eq2* (Figure 5 (a)). This oscillating behavior translates into a net flux of component 2 that is first directed towards the vapor-liquid interface ($j_2 > 0$), but then, for a short period in time, goes in the reverse direction ($j_2 < 0$), to then turn back to the expected direction again ($j_2 > 0$) (Figure 5 (c)). The negative flux of j_2 can be interpreted as a reflection of particles of component 2 at the vapor-liquid interface, i.e. an important part of the particles of component 2 that are reaching the interface cannot enter the liquid phase. This is related to several effects: firstly, the low solubility of component 2 in the liquid phase of mixture A, that obviously hinders the uptake of component 2 by the liquid phase, and, secondly, the enrichment that builds up in the interfacial region in mixture A, as will be discussed below in more detail. The low affinity of the liquid phase to component 2 in mixture A is a consequence of the choice of the molecular parameters (low values of ε_2 and ξ_{12} for mixture A). In the discussion of the decay of the signals for mixture B, we have mentioned a slight change at about $\tau = 1,200\,\sigma(m/\varepsilon)^{1/2}$. This could be due to a similar effect as the one observed for mixture A, which, however, is much milder for mixture B, as the solubility of component 2 in the liquid phase is much better for that mixture.

The fact that particles can be repelled from a vapor-liquid interface has been reported by previously Garret et al.[66], who considered, however, equilibrium conditions, in which they tracked individual particles (e.g. OH and O_3 radicals at water-air interfaces[85,86]). To the best of our knowledge, this effect has never before been observed in mass transfer studies. Due to the symmetry of the overall simulation scenario, the repelled particles are once again repelled at the symmetry plane in the middle of the vapor phase, which could explain the small oscillations that were observed mainly in the signal for the flux j_2 in the vapor phase measurement volume $\mathrm{MV}_{\mathrm{vap}}$ (Figure 5 (c)).

Figure 6 shows the transient response in the pressure-composition diagram at $T = 0.715\,\varepsilon k_{\mathrm{B}}^{-1}$ for both studied mixtures. The pressure sampled in the liquid and vapor measurement volume is shown as a function of composition x_2 and time τ. The liquid and vapor phase state points of both *Eq1* (before the insertion) and *Eq2* (after the insertion and relaxation) have the same pressure, as expected in a vapor-liquid equilibrium. The *Eq1* and *Eq2* points of the vapor and liquid domain agree well with the dew and bubble lines calculated with the PeTS EOS[10,80]. The pressure sampled in the liquid phase has high noise compared to data from the vapor phase, which is typical for pressure sampled in liquid phases (cf. Figure 5 (e) and (f)).

2. Response at the Vapor-Liquid Interface

Figure 7 shows spatial profiles of the density ρ_2 and the molar flux j_2 of component 2 in the vicinity of the interface and the neighboring bulk phases for both mixtures at $T = 0.715\,\varepsilon k_\mathrm{B}^{-1}$. The spatial profiles are discretized in time with an interval of $\Delta\tau = 100\,\sigma(m/\varepsilon)^{1/2}$. The measured spatial profiles for each time step were superimposed at the interface position $z_{50}(\tau)$ to decrease the influence from fluctuations of that position. The *In* phase starts at $\tau = 1,000\,\sigma(m/\varepsilon)^{1/2}$. The profiles measured before this time are essentially identical and represent the initial equilibrium state *Eq1*, in which no component 2 is present.

We will discuss the results for mixture B first. For that mixture, a temporary density peak of component 2 builds up in the interfacial region, cf. Figure 7 (b). Within the interfacial region, which is basically determined here by density profiles of component 1 (cf. Section II B), this peak is shifted towards the liquid side of the interface. At about $\tau = 1,400\,\sigma(m/\varepsilon)^{1/2}$, this temporary density peak reaches its maximum height and then decays and finally vanishes in the equilibrium density profile of component 2 for the equilibrium state *Eq2*, that shows no extrema.

The temporary density peak of component 2 at the interface for mixture B can be interpreted as a kind of jamming. The insertion of the particles of component 2 creates an important flux j_2 in the vapor phase that is directed towards the interface. There is only little friction in the gas phase, so the particles of component 2 reach the interface with a high directed velocity. At the interface, they are slowed down by the particles in the liquid. The transport of component 2 in the liquid phase is diffusion-controlled and slower than the gas phase transport. This leads to a temporary accumulation of component 2 near the interface, which, however, vanishes as the overall transport goes to zero upon approaching the equilibrium state *Eq2*.

For mixture B, the molar flux j_2 is positive at all times and all locations as expected (the flux is always directed from the gas phase to the liquid phase). However, the flux is far from being uniform in the volume shown in Figure 7, which extends $10\,\sigma$ to both sides of the vapor-liquid interface. The flux j_2 measured on the vapor side shortly after the insertion are very large, but they decay quickly ($\tau < 500\,\sigma(m/\varepsilon)^{1/2}$) by almost an order of magnitude of the process. The further decay to zero is then slower.

In interpreting the j_2-flux curves, it has to be considered, that a negative slope in the profile shown in Figure 7 indicates that component 2 accumulates over time in the considered element, a constant profile indicates a steady state, and a positive slope indicates depletion. In general, as expected, a depletion is observed on the vapor side and an accumulation on the liquid side (disregarding the details related to the build-up and vanishing of the density peak discussed above). The exception is the profile measured at $\tau = 1,100\,\sigma(m/\varepsilon)^{1/2}$ on the vapor side where an accumulation is observed, which is due to the fact that the insertion phase just stopped.

Also for mixture A, a peak builds up in the concentration profile of component 2 near the interface shortly after the insertion phase *In* is finished. But this peak in mixture A is of different nature than the one in mixture B – it does not vanish and persists also in the equilibrium state *Eq2*. The peak observed in mixture A is caused by the well-known enrichment of light-boiling components at vapor-liquid equilibrium interfaces[1–13], which is known to be important for mixture A, but not for mixture B[10,72]. In mixture A, the enrichment peak builds up very quickly (in about $200\,\sigma(m/\varepsilon)^{1/2}$) and then undergoes only minor changes during the rest of the process (it diminishes slightly, but the difference between the maximal height and the end height are only of the order of 10 %). In contrast to the peak observed in mixture B, the enrichment peak in mixture A is almost symmetric with respect to the interface, which confirms previous findings[72].

The flux j_2 measured in mixture A shortly after the end of the insertion period *In* (at $\tau = 1,100\,\sigma(m/\varepsilon)^{1/2}$) is similar to that measured in mixture B, which is not unexpected, as the disturbance is then still limited largely to the vapor phase. However, for larger times, major differences occur. First, the flux j_2 is much lower for mixture A than for mixture B, which can be interpreted as a consequence of the lower solubility of component 2 in the liquid in mixture A. Furthermore, it can be seen that at $\tau = 1,200\,\sigma(m/\varepsilon)^{1/2}$ the flux j_2 is reversed in the vapor phase, i.e. there is a net flow of component 2 from the surface back to the vapor. This effect has been discussed already above and is interpreted as a reflection of particles of component 2 at the interface. It may be associated to the build-up of the interfacial enrichment.

The temporary density peak of mixture B at the interface position might also be caused by a higher solubility due to the increased pressure. The bubble line of mixture B has a flat positive slope (cf. Figure 6 right). Hence, an increase in pressure significantly increases the mole fraction of component 2 in the liquid phase of mixture B in an equilibrium state, i.e. the solubility of component 2 in the liquid phase increases. The pressure in the vapor phase of mixture B is higher than the pressure of the second equilibrium state *Eq2* up to $\tau = 1,700\,\sigma(m/\varepsilon)^{1/2}$, cf. Figure 5 (d), while the density peak builds up until $\tau = 1,400\,\sigma(m/\varepsilon)^{1/2}$, cf. Figure 7 (b). The temporarily increased pressure raises the solubility of component 2, which in turn increases the molar flux across the interface and causes the temporary density peak. In contrast, the slope of the bubble line of mixture A is positive and very steep (cf. Figure 6 left). An increase in pressure only slightly increases the mole fraction of the liquid phase of mixture A in an equilibrium state. Mixture A shows only a slight temporary increased density at the interface, cf. Figure 7 (a).

B. Results for Various Temperatures

The new simulation method was not only used to study the mass transfer process in mixture A and mixture B at the temperature $T = 0.715\,\varepsilon k_{\mathrm{B}}^{-1}$ but also at the temperatures $T = 0.66, 0.77, 0.825\,\varepsilon k_{\mathrm{B}}^{-1}$. This is of particular interest since the interfacial properties of the mixtures are known to depend strongly on the temperature[10,71], e.g. the enrichment of mixture A is known to decrease with increasing temperature.

Figure 8 shows the results for the density of component 2 as a function of time sampled in the measurement volumes in the vapor phase ($\mathrm{MV_{vap}}$, top) and liquid phase ($\mathrm{MV_{liq}}$, bottom) for both mixtures A and B, for all studied temperatures. In all cases, the change in temperature leads to quantitative changes, but the qualitative behavior is the same for all temperatures, which is not unexpected. Overall, the influence of the temperature on the results is larger for mixture B, mainly as the solubility of component 2 in the liquid depends on temperature for that mixture, whereas it is hardly temperature-dependent for mixture A, cf. Figure 8 (c).

It is interesting to note that, contrary to the overall trend, the height of the initial peak in the density ρ_2 measured in the vapor phase ($\mathrm{MV_{vap}}$) in mixture A depends strongly on temperature: the peak is large for low temperatures and almost vanishes at the highest studied temperature. Together with the fact that the solubility of component 2 in the liquid phase is hardly temperature-dependent, this is a strong argument for the influence of the enrichment on this peak, namely as the enrichment is known to be high at low temperatures and vice versa[10,71]. This argument is further supported by the findings for mixture B for the density ρ_2 in $\mathrm{MV}_{\mathrm{vap}}$, where the influence of the temperature on the peak height is quite low, despite the considerable influence on temperature on the solubility.

Figure 8 shows the flux of component 2 sampled at different positions in the simulation box as a function of time in replica simulations at various temperatures for mixture A (left) and mixture B (right). Results for three positions are reported: the measurement volume on the vapor side ($\mathrm{MV}_{\mathrm{vap}}$), the interfacial plane ($z = z_{50}$, see Section II B), and the measurement volume on the liquid side ($\mathrm{MV}_{\mathrm{liq}}$). The results confirm that the variation of the temperature leads to quantitative changes, but the qualitative behavior remains the same. Differences in the flux of component 2 caused by a variation of the temperature are mainly limited to the first peak in the flux observed shortly after the insertion phase. In remarkable agreement, in basically all cases shown in Figure 8, the peak is highest for the lowest temperature and its height decreases steadily with increasing temperature. The only exception from this rule is the density signal from the liquid side $\mathrm{MV}_{\mathrm{liq}}$ for mixture A, which, albeit, exhibits only a very small peak.

Additional results for the temperature dependency of the transient response are given in the Supporting Information.

V. CONCLUSIONS

A non-stationary molecular dynamics simulation method is introduced for studying mass transfer through vapor-liquid interfaces. The mass transfer of a certain component through the interface is driven by a concentration gradient of the respective component that is initially build up and then the system relaxes in a new equilibrium state. During that relaxation process, the mass transfer through the vapor-liquid interface is examined in detail. The statistics of the sampling of the observables is amplified by studying sets of simulation replicas, which only differ in their initial velocity distribution.

In the proposed simulation method, particles of component 2 are inserted in the middle of the vapor phase of an equilibrated vapor-liquid system containing only particles of component 1 over a short period of time. After the insertion phase, the system is re-equilibrated. During this relaxation phase, the inserted particles move from the vapor phase through the vapor-liquid interface and enter the liquid phase. Over the whole simulation run, profiles of the density, composition, and mass flux of each component as well as the pressure are sampled.

The simulation method was tested on binary mixtures of simple fluids. Two binary LJTS mixtures with the same high-boiling component and different low-boiling components were investigated. Both mixtures show distinctly different phase behaviors and interfacial properties such as the enrichment[10,71], while having a comparable bulk diffusivity[22]. Mixture A shows a high enrichment, while mixture B shows none. The number of inserted particles is chosen the same for the two studied mixtures. Even though both mixtures have similar bulk phase diffusivities, the results from both mixtures from the new simulation method are distinctly different, which can be attributed to differences in the interfacial properties. The behavior of the mass flux across the interface deviates significantly between the two studied mixtures: For mixture A, an important part of the particles are repelled at the interface. The repulsion of particles at the interface causes a temporarily negative net flux back into the vapor phase. No temporary negative flux is observed for mixture B. For mixture B, on the other hand, a temporary density peak is observed at the beginning of the relaxation process on the liquid side of the interface. This temporary accumulation of component 2 particles at the interface is caused by jamming due to a lower transport resistance at the interface and in the liquid bulk phase compared to the vapor bulk phase. The different behavior of mixture A and B is attributed to three facts: (i) the mass transfer process is governed by the bulk properties of the second equilibrium state, which in turn is dependent on the number of inserted particles and of course the mixture, (ii) a significant amount of particles of component 2 is repelled at the interface in the case of mixture A; (iii) the enrichment acts as a mass transfer resistance. Yet, the significance of the last two phenomena have to be evaluated in further studies.

The results from this work strongly support the hypothesis that interfacial properties influence the mass transfer through fluid interfaces. The resistance to mass transfer at the interface is a dynamic property and can eventually become high enough to temporary reduce or completely stop flux through the interface and accordingly particles are repelled at the interface. The non-stationary simulation method proposed in this work is a valuable tool for further investigations, e.g. for studying real substance mixtures and liquid-liquid interfaces.

ACKNOWLEDGMENTS

The authors gratefully acknowledge funding of the present work by the ERC Advanced Grant ENRICO (grant agreement No. 694807). The present work was conducted under the auspices of the Boltzmann-Zuse Society of Computational Molecular Engineering (BZS) and the simulations were carried out on the Regional University Computing Center Kaiserslautern (RHRK) under the grant TUK-MTD as well as the Leibniz Supercomputing Centre (LRZ) under the grant $(\mathrm{AMSEL})^2$ (pn56mo).

TABLES & FIGURES

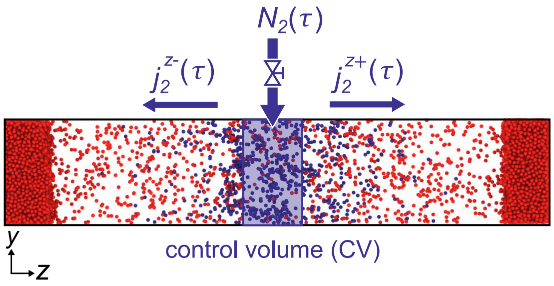

FIG. 1: Scheme of the non-stationary simulation scenario. The snapshot is taken from a simulation during the insertion phase. Prior to the insertion, the system contains only particles of the high-boiling component 1 (red). Particles of component 2 (blue) are inserted into the control volume (blue shaded area), then spread through the vapor phase, cross the vapor-liquid interface, and enter into the liquid phase until a new equilibrium state is established.

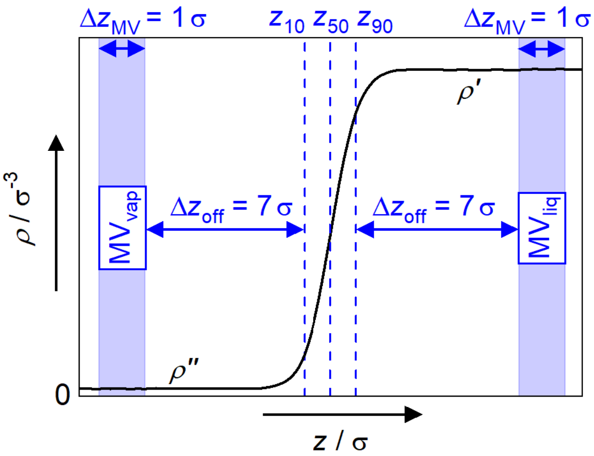

FIG. 2: Schematic of the geometric configuration of the measurement volumes (MV) located in the vicinity of the interface; showing the total density at the interface as a function of the z-direction (—). The vapor and liquid measurement volume (blue shaded areas) are located at a distance of $\Delta z_{\mathrm{off}} = 7\,\sigma$ to the characteristic interface points z_{10} and z_{90}, respectively. The positions z_{10}, z_{50} and z_{90} (---) are defined according to Eq. (1).

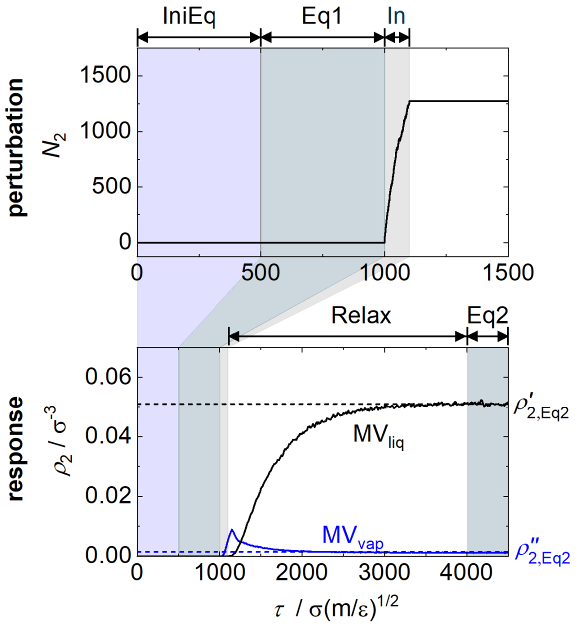

FIG. 3: Example for results from the evaluation of a set of replicas of simulation runs used here for illustrating the simulation phases. Top: number of inserted particles of component 2 N_2 as a function of the simulation time (perturbation of the system); Bottom: density of component 2 in the measurement volumes $\mathrm{MV_{vap}}$ and $\mathrm{MV_{liq}}$ (cf. Figure 2) as a function of the simulation time (response of the system). The dashed lines indicate the equilibrium states at the end of the relaxation (*Eq2*).

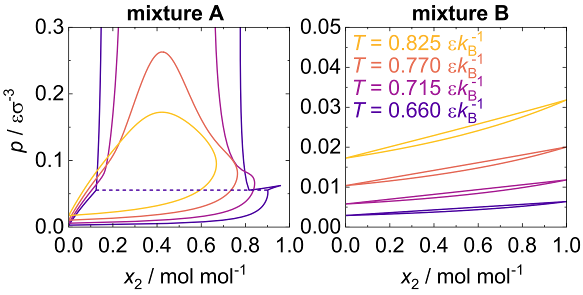

FIG. 4: Phase diagrams of mixture A (left) and mixture B (right) for all investigated temperatures calculated with the PeTS EOS[10,80].

TABLE I: Selected input parameters and results from the NEMD simulations for mixtures A and B carried out in the present work. Input: the temperature T in the whole simulation box and the chemical potential $\mu_{2,\mathrm{CV}}$ in the control volume during insertion phase. Results: the number of inserted particles N_2 as well as vapor-liquid equilibrium properties for the initial and the final state: Pressure p and partial density of component 2 ρ_2 in the vapor phase ($''$) and the liquid phase ($'$). The uncertainty is reported in parentheses and refers to the last digits of the value. It was obtained from the standard deviation from the results from the simulations of the set of replicas.

Mixture	T / $\varepsilon k_\mathrm{B}^{-1}$	$\mu_{2,\mathrm{CV}}$ / ε	N_2	p''_Eq1 / $\varepsilon\sigma^{-3}$	p''_Eq2 / $\varepsilon\sigma^{-3}$	$\rho''_{2,\mathrm{Eq2}}$ / σ^{-3}	$\rho'_{2,\mathrm{Eq2}}$ / σ^{-3}
A	0.66	-0.55	1189(43)	0.0030(1)	0.0086(3)	0.0088(4)	0.0106(15)
	0.715	-0.675	1199(46)	0.0058(2)	0.0122(3)	0.0092(4)	0.0104(11)
	0.77	-0.8	1195(44)	0.0105(2)	0.0175(4)	0.0094(4)	0.0105(8)
	0.825	-0.9	1204(45)	0.0173(3)	0.0252(4)	0.0097(5)	0.0105(8)
B	0.66	-0.8	1194(66)	0.0030(1)	0.0032(1)	0.0007(1)	0.0538(26)
	0.715	-0.9	1212(64)	0.0059(2)	0.0063(2)	0.0011(1)	0.0519(26)
	0.77	-1.025	1189(65)	0.0105(2)	0.0111(2)	0.0018(2)	0.0485(26)
	0.825	-1.15	1184(59)	0.0173(3)	0.0183(4)	0.0026(2)	0.0455(23)

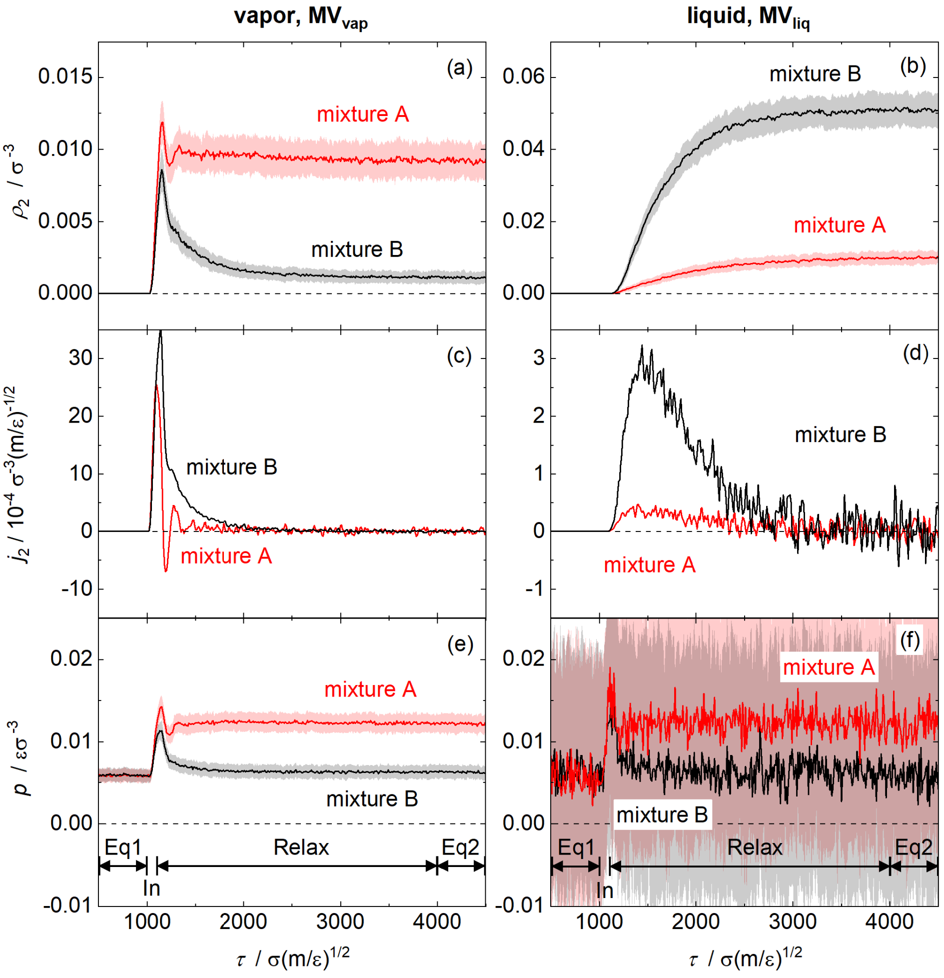

FIG. 5: Observables sampled in the replica NEMD simulations in the measurement volumes in the vapor phase MV$_{\mathrm{vap}}$ (left) and in the liquid phase MV$_{\mathrm{liq}}$ (right), respectively, as a function of the simulation time: density of component 2 ρ_2, flux of component 2 j_2, and pressure p. The temperature was $T = 0.715\,\varepsilon k_{\mathrm{B}}^{-1}$. Results for mixtures A are indicated in red; results for mixtures B in black. Solid lines indicate the mean value obtained from the set of replicas, the shaded area indicates standard deviation. The standard deviation is only given for the two properties that were sampled directly (ρ_2 and p); j_2 was calculated from ρ_2.

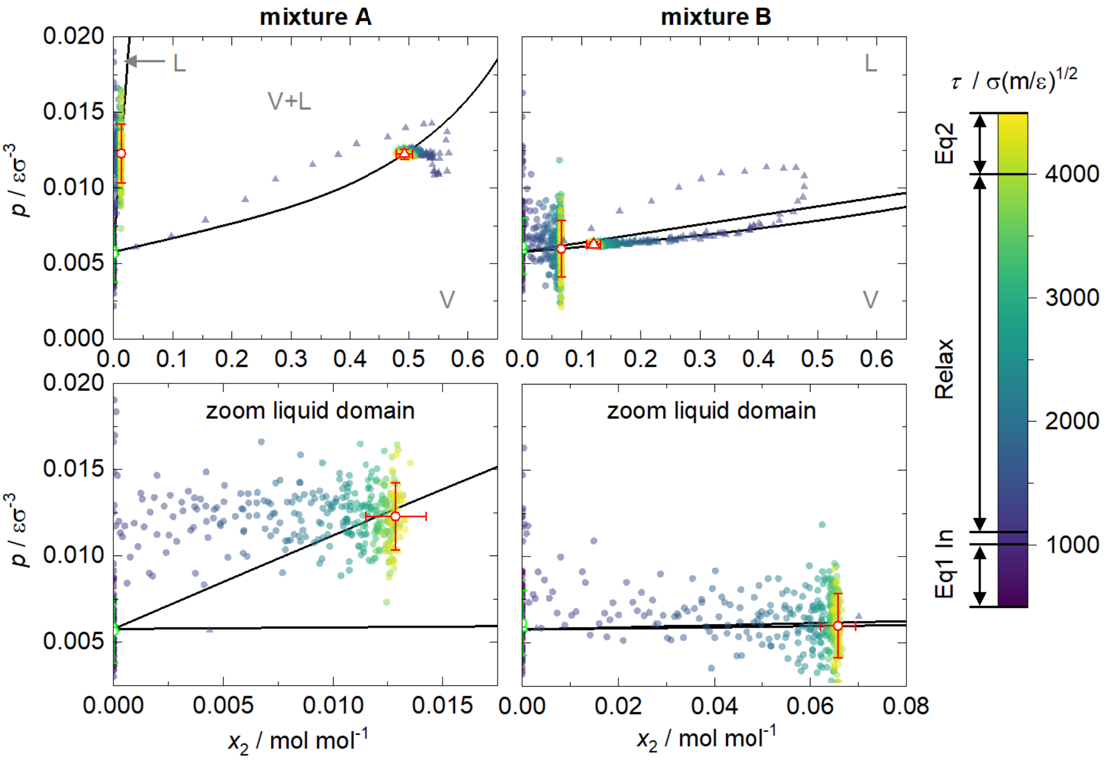

FIG. 6: Pressure-composition diagram at $T = 0.715\,\varepsilon k_\mathrm{B}^{-1}$ for mixtures A (left) and mixtures B (right). Circles indicate state points sampled in the measurement volume $\mathrm{MV_{liq}}$; triangles indicate state points sampled in the measurement volume $\mathrm{MV_{vap}}$. The bottom plots give a detailed view on the state points sampled in the liquid phase. The color scale indicates the simulation time. Each data point represents the mean value obtained from a set of replicas at a given simulation time τ. The white filled symbols indicate pressure and composition in *Eq1* (green) and in *Eq2* (red) phase. The error bars are the standard deviation obtained from a set of replicas. The black line indicates the phase equilibrium computed with the PeTS EOS[10,80].

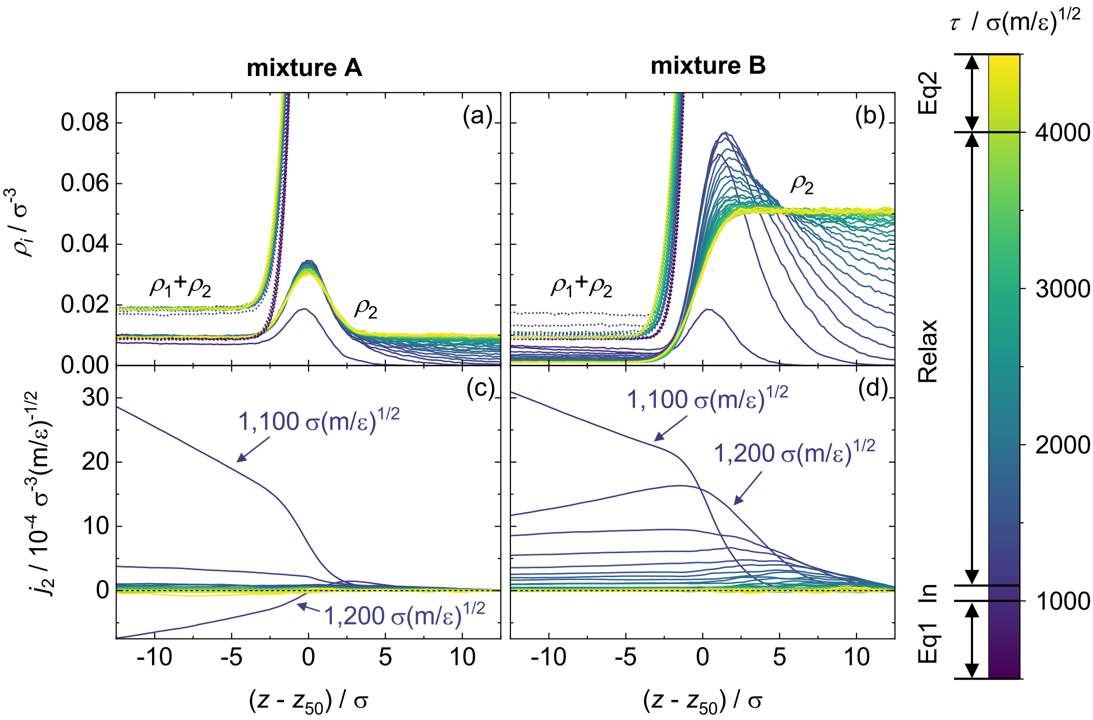

FIG. 7: Spatial profiles of the observables sampled in the vicinity of the interface and the neighboring bulk phases for mixture A (left) and mixture B (right). Results for the temperature $T = 0.715\,\varepsilon k_\mathrm{B}^{-1}$ from replica simulations. Top: density of the low-boiling component 2 (—) and total density (·····); Bottom: molar flux of component 2 j_2. The simulation time τ is indicated by the color. The shown profiles were measured at time intervals of $\Delta\tau = 100\,\sigma(m/\varepsilon)^{1/2}$.

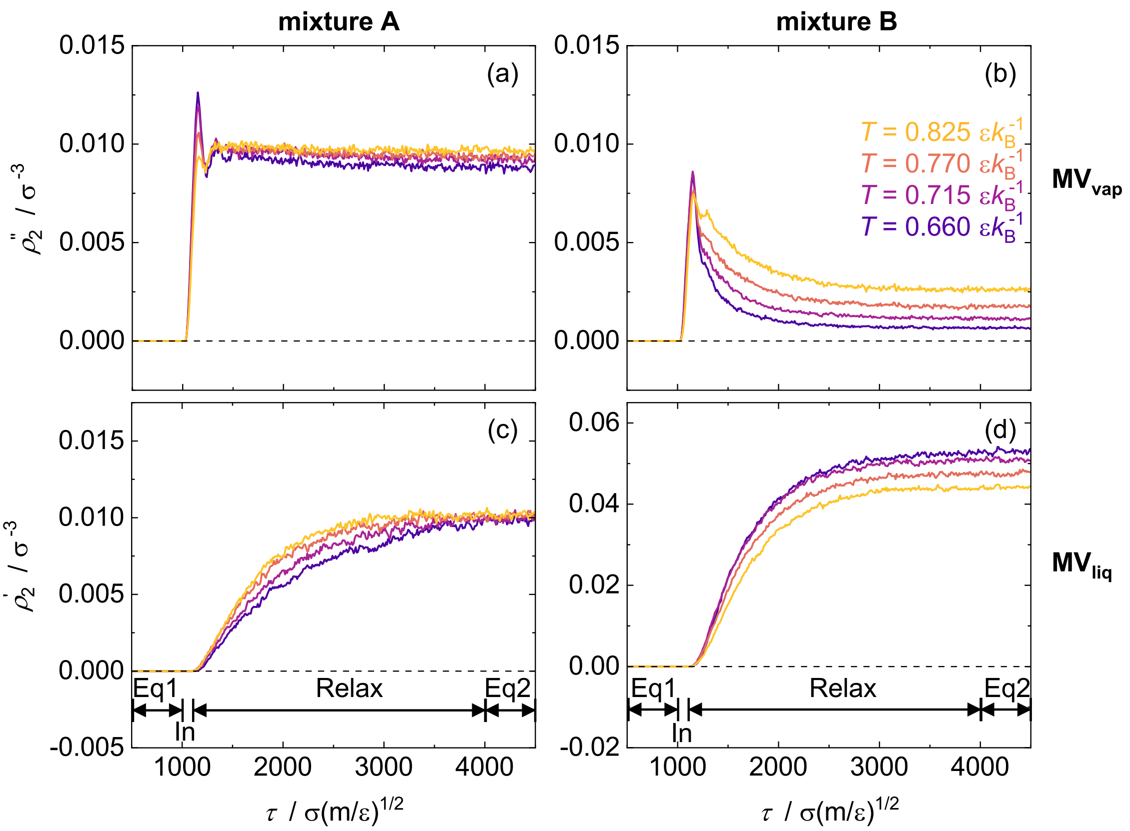

FIG. 8: Density of component 2 sampled in the measurement volume in the vapor phase MV_{vap} (top) and in the measurement volume in the liquid phase MV_{liq} (bottom) as a function of the simulation time τ. Results for mixture A (left) and mixture B (right) from replica simulations at different temperatures are shown, which are indicated by color.

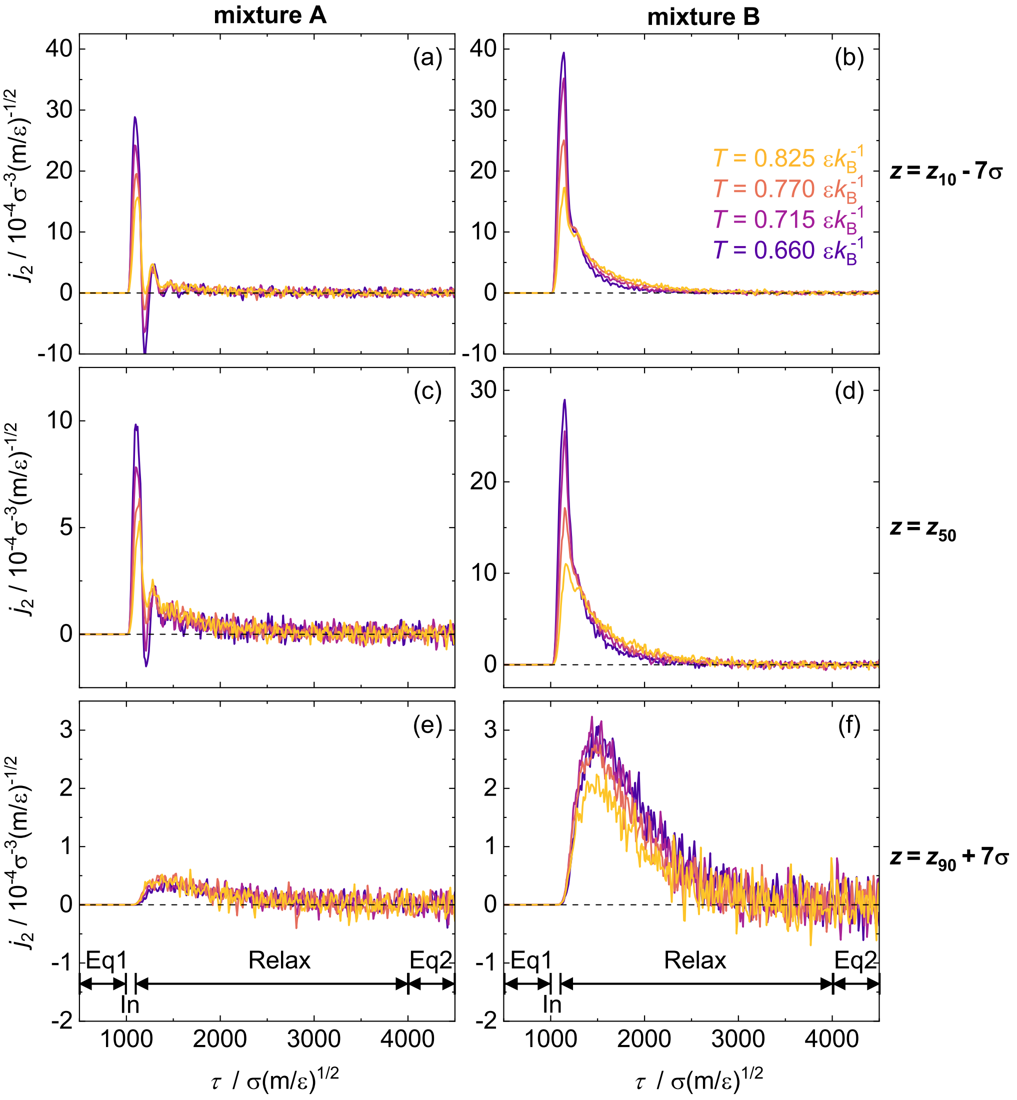

FIG. 9: Molar flux of component 2 sampled at different positions as a function of time in replica simulations at different temperatures for mixture A (left) and mixture B (right). The temperature is represented by the color. Top: measurement volume on the vapor side ($\mathrm{MV_{vap}}$); Middle: interface plane $z = z_{50}$, Bottom: measurement volume on the liquid side ($\mathrm{MV_{liq}}$).

REFERENCES

[1] S. Becker, S. Werth, M. Horsch, K. Langenbach, and H. Hasse, "Interfacial tension and adsorption in the binary system ethanol and carbon dioxide: Experiments, molecular simulation and density gradient theory," Fluid Phase Equilibria **427**, 476 (2016).

[2] W. Li and Z. Jin, "Molecular dynamics simulation of natural gas-water interfacial tensions over wide range of pressures," Fuel **236**, 480–492 (2019).

[3] W. A. Fouad and L. F. Vega, "The phase and interfacial properties of azeotropic refrigerants: the prediction of aneotropes from molecular theory," Physical Chemistry Chemical Physics **19**, 8977–8988 (2017).

[4] O. G. Niño-Amézquita, D. van Putten, and S. Enders, "Phase equilibrium and interfacial properties of water+CO_2 mixtures," Fluid Phase Equilibria **332**, 40 (2012).

[5] O. G. Niño-Amézquita and S. Enders, "Phase equilibrium and interfacial properties of water+methane mixtures," Fluid Phase Equilibria **407**, 143–151 (2016).

[6] F. Llovell, N. M. Dowell, F. J. Blas, A. Galindo, and G. Jackson, "Application of the SAFT-VR density functional theory to the prediction of the interfacial properties of mixtures of relevance to reservoir engineering," Fluid Phase Equilibria **336**, 137–150 (2012).

[7] S. Enders and H. Kahl, "Interfacial properties of water + alcohol mixtures," Fluid Phase Equilibria **263**, 160–167 (2008).

[8] T.-M. Chang and L. X. Dang, "Liquid-vapor interface of methanol-water mixtures: A molecular dynamics study," The Journal of Physical Chemistry B **109**, 5759–5765 (2005).

[9] A. H. Falls, L. E. Scriven, and H. T. Davis, "Adsorption, structure, and stress in binary interfaces," The Journal of Chemical Physics **78**, 7300–7317 (1983).

[10] S. Stephan, K. Langenbach, and H. Hasse, "Interfacial properties of binary Lennard-Jones mixtures by molecular simulations and density gradient theory," The Journal of Chemical Physics **150**, 174704 (2019).

[11] S. Stephan, S. Becker, K. Langenbach, and H. Hasse, "Vapor-liquid interfacial properties of the system cyclohexane+ CO_2: Experiments, molecular simulation and density gradient theory," Fluid Phase Equilibria **518**, 112583 (2020).

[12] E. A. Müller and A. Mejía, "Interfacial properties of selected binary mixtures containing n-alkanes," Fluid Phase Equilibria **282**, 68–81 (2009).

[13] C. Miqueu, J. M. Miguez, M. M. Piñeiro, T. Lafitte, and B. Mendiboure, "Simultaneous

application of the gradient theory and Monte Carlo molecular simulation for the investigation of methane/water interfacial properties," The Journal of Physical Chemistry B **115**, 9618–9625 (2011).

[14]S. Stephan, H. Cárdenas, A. Mejía, and E. A. Müller, "The monotonicity behavior of density profiles at vapor-liquid interfaces of mixtures," Fluid Phase Equilibria **564**, 113596 (2023).

[15]R. Nagl, P. Zimmermann, and T. Zeiner, "Interfacial mass transfer in water-toluene systems," Journal of Chemical & Engineering Data **2**, 328–336 (2020).

[16]S. Stephan, K. Langenbach, and H. Hasse, "Enrichment of components at vapour-liquid interfaces: A study by molecular simulation and density gradient theory," Chemical Engineering Transactions **69**, 295–300 (2018).

[17]C. Klink and J. Gross, "A density functional theory for vapor-liquid interfaces of mixtures using the perturbed-chain polar statistical associating fluid theory equation of state," Industrial & Engineering Chemistry Research **53**, 6169–6178 (2014).

[18]D. J. Lee, M. M. Telo da Gama, and K. E. Gubbins, "The vapour-liquid interface for a Lennard-Jones model of argon-krypton mixtures," Molecular Physics **53**, 1113–1130 (1984).

[19]M. M. Telo da Gama and R. Evans, "The structure and surface tension of the liquid-vapour interface near the upper critical end point of a binary mixture of Lennard-Jones fluids I. the two phase region," Molecular Physics **48**, 229–250 (1983).

[20]J. M. Garrido, M. M. Piñeiro, A. Mejía, and F. J. Blas, "Understanding the interfacial behavior in isopycnic Lennard-Jones mixtures by computer simulations," Physical Chemestry Chemical Physics **18**, 1114–1124 (2016).

[21]B. Karlsson and R. Friedman, "Dilution of whisky - the molecular perspective," scientific reports **7**, 1–9 (2017).

[22]S. Stephan, D. Schaefer, K. Langenbach, and H. Hasse, "Mass transfer through vapour–liquid interfaces: a molecular dynamics simulation study," Molecular Physics **119**, e1810798 (2021).

[23]M. Heinen, J. Vrabec, and J. Fischer, "Communication: Evaporation: Influence of heat transport in the liquid on the interface temperature and the particle flux," The Journal of Chemical Physics **145**, 081101 (2016).

[24]A. Lotfi, J. Vrabec, and J. Fischer, "Evaporation from a free liquid surface," International

Journal of Heat and Mass Transfer **73**, 303 (2014).

[25]S. Homes, M. Heinen, J. Vrabec, and J. Fischer, "Evaporation driven by conductive heat transport," Molecular Physics **119**, e1836410 (2020).

[26]R. S. Chatwell, M. Heinen, and J. Vrabec, "Diffusion limited evaporation of a binary liquid film," International Journal of Heat and Mass Transfer **132**, 1296–1305 (2019).

[27]M. Heinen and J. Vrabec, "Evaporation sampled by stationary molecular dynamics simulation," The Journal of Chemical Physics **151**, 044704 (2019).

[28]T. Tsuruta, H. Tanaka, and T. Masuoka, "Condensation/evaporation coefficient and velocity distributions at liquid–vapor interface," International Journal of Heat and Mass Transfer **42**, 4107–4116 (1999).

[29]S. Cheng, J. B. Lechman, S. J. Plimpton, and G. S. Grest, "Evaporation of Lennard-Jones fluids," The Journal of Chemical Physics **134**, 224704 (2011).

[30]J. M. Simon, D. Bedeaux, S. Kjelstrup, J. Xu, and E. Johannessen, "Interface film resistivities for heat and mass transfersintegral relations verified by non-equilibrium molecular dynamics," The Journal of Physical Chemistry B **110**, 18528–18536 (2006).

[31]J. Ge, D. Bedeaux, J. Simon, and S. Kjelstrup, "Integral relations, a simplified method to find interfacial resistivities for heat and mass transfer," Physica A: Statistical Mechanics and its Applications **385**, 421–432 (2007).

[32]J. Ge, S. Kjelstrup, D. Bedeaux, J. M. Simon, and B. Rousseau, "Transfer coefficients for evaporation of a system with a Lennard-Jones long-range spline potential," Phys. Rev. E **75**, 061604 (2007).

[33]M. Matsumoto, "Molecular dynamics simulation of interphase transport at liquid surfaces," Fluid Phase Equilibria **125**, 195–203 (1996).

[34]A. Kryukov and V. Levashov, "About evaporation–condensation coefficients on the vapor–liquid interface of high thermal conductivity matters," International Journal of Heat and Mass Transfer **54**, 3042 – 3048 (2011).

[35]M. Kon, K. Kobayashi, and M. Watanabe, "Kinetic boundary condition in vapor–liquid two-phase system during unsteady net evaporation/condensation," European Journal of Mechanics - B/Fluids **64**, 81–92 (2017).

[36]E. Bird and Z. Liang, "Transport phenomena in the Knudsen layer near an evaporating surface," Phys. Rev. E **100**, 043108 (2019).

[37]S. Kjelstrup and B. Hafskjold, "Nonequilibrium molecular dynamics simulations of steady-

state heat and mass transport in distillation," Industrial & Engineering Chemistry Research **35**, 4203–4213 (1996).

[38] A. Røsjorde, S. Kjelstrup, D. Bedeaux, and B. Hafskjold, "Nonequilibrium Molecular Dynamics Simulations of Steady-State Heat and Mass Transport in Condensation. II. Transfer Coefficients," Journal of Colloid and Interface Science **240**, 355–364 (2001).

[39] A. Røsjorde, D. Fossmo, D. Bedeaux, S. Kjelstrup, and B. Hafskjold, "Nonequilibrium molecular dynamics simulations of steady-state heat and mass transport in condensation: I. local equilibrium," Journal of Colloid and Interface Science **232**, 178–185 (2000).

[40] I. Inzoli, S. Kjelstrup, D. Bedeaux, and J. Simon, "Transfer coefficients for the liquid–vapor interface of a two-component mixture," Chemical Engineering Science **66**, 4533–4548 (2011).

[41] B. Hafskjold and T. Ikeshoji, "Non equilibrium molecular dynamics simulation of coupled heat- and mass transport across a liquid/vapor interface," Molecular Simulation **16**, 139–150 (1996).

[42] L. van der Ham, R. Bock, and S. Kjelstrup, "Modelling the coupled transfer of mass and thermal energy in the vapour–liquid region of a nitrogen–oxygen mixture," Chemical Engineering Science **65**, 2236–2248 (2010).

[43] E. Johannessen, J. Gross, and D. Bedeaux, "Nonequilibrium thermodynamics of interfaces using classical density functional theory," The Journal of Chemical Physics **129**, 184703 (2008).

[44] E. Johannessen and D. Bedeaux, "Integral relations for the heat and mass transfer resistivities of the liquid–vapor interface," Physica A: Statistical Mechanics and its Applications **370**, 258–274 (2006).

[45] K. Glavatskiy and D. Bedeaux, "Transport of heat and mass in a two-phase mixture: From a continuous to a discontinuous description," The Journal of Chemical Physics **133**, 144709 (2010).

[46] C. Klink, C. Waibel, and J. Gross, "Analysis of interfacial transport resistivities of pure components and mixtures based on density functional theory," Industrial & Engineering Chemistry Research **54**, 11483–11492 (2015).

[47] M. Lísal, J. K. Brennan, W. R. Smith, and F. R. Siperstein, "Dual control cell reaction ensemble molecular dynamics: A method for simulations of reactions and adsorption in porous materials," The Journal of Chemical Physics **121**, 4901–4912 (2004).

[48] G. Arya, H.-C. Chang, and E. J. Maginn, "A critical comparison of equilibrium, non-equilibrium and boundary-driven molecular dynamics techniques for studying transport in microporous materials," The Journal of Chemical Physics **115**, 8112–8124 (2001).

[49] Z. Ható, D. Boda, and T. Kristóf, "Simulation of steady-state diffusion: Driving force ensured by dual control volumes or local equilibrium monte carlo," The Journal of Chemical Physics **137**, 054109 (2012).

[50] M. G. Martin, A. P. Thompson, and T. M. Nenoff, "Effect of pressure, membrane thickness, and placement of control volumes on the flux of methane through thin silicalite membranes: A dual control volume grand canonical molecular dynamics study," The Journal of Chemical Physics **114**, 7174–7181 (2001).

[51] P. Pohl, G. S. Heffelfinger, and D. M. Smith, "Molecular dynamics computer simulation of gas permeation in thin silicalite membranes," Molecular Physics **89**, 1725–1731 (1996).

[52] P. I. Pohl and G. S. Heffelfinger, "Massively parallel molecular dynamics simulation of gas permeation across porous silica membranes," Journal of Membrane Science **155**, 1–7 (1999).

[53] J. M. D. MacElroy, "Nonequilibrium molecular dynamics simulation of diffusion and flow in thin microporous membranes," The Journal of Chemical Physics **101**, 5274–5280 (1994).

[54] A. P. Thompson, D. M. Ford, and G. S. Heffelfinger, "Direct molecular simulation of gradient-driven diffusion," The Journal of Chemical Physics **109**, 6406–6414 (1998).

[55] A. P. Thompson and G. S. Heffelfinger, "Direct molecular simulation of gradient-driven diffusion of large molecules using constant pressure," The Journal of Chemical Physics **110**, 10693–10705 (1999).

[56] J. Sun and L. T. Zhang, "Temperature control algorithms in dual control volume grand canonical molecular dynamics simulations of hydrogen diffusion in palladium," The Journal of Chemical Physics **127**, 164721 (2007).

[57] G. S. Heffelfinger and F. van Swol, "Diffusion in Lennard-Jones fluids using dual control volume grand canonical molecular dynamics simulation (DCV-GCMD)," The Journal of Chemical Physics **100**, 7548–7552 (1994).

[58] G. S. Heffelfinger and D. M. Ford, "Massively parallel dual control volume grand canonical molecular dynamics with LADERA I. gradient driven diffusion in Lennard-Jones fluids," Molecular Physics **94**, 659–671 (1998).

[59] G. Heffelfinger and D. Ford, "Massively parallel dual control volume grand canonical molec-

ular dynamics with LADERA II. gradient driven diffusion through polymers," Molecular Physics **94**, 673–683 (1998).

[60] P. M. Rauscher, H. C. Öttinger, and J. J. de Pablo, "Nonequilibrium statistical thermodynamics of multicomponent interfaces," Proceedings of the National Academy of Sciences **119**, e2121405119 (2022).

[61] V. G. Baidakov, S. P. Protsenko, and V. M. Bryukhanov, "Relaxation processes at liquid-gas interfaces in one- and two-component Lennard-Jones systems: Molecular dynamics simulation," Fluid Phase Equilibria **481**, 1 – 14 (2019).

[62] V. G. Baidakov and S. P. Protsenko, "Molecular-dynamics simulation of relaxation processes at liquid–gas interfaces in single- and two-component Lennard-Jones systems," Colloid Journal **81**, 491–500 (2019).

[63] K. Bucior, L. Yelash, and K. Binder, "Molecular-dynamics simulation of evaporation processes of fluid bridges confined in slitlike pores," Physical Review E **79**, 031604 (2009).

[64] C. Braga, A. Galindo, and E. A. Müller, "Nonequilibrium molecular dynamics simulation of diffusion at the liquid-liquid interface," The Journal of Chemical Physics **141**, 154101 (2014).

[65] C. Braga, J. Muscatello, G. Lau, E. A. Müller, and G. Jackson, "Nonequilibrium study of the intrinsic free-energy profile across a liquid-vapour interface," The Journal of Chemical Physics **144**, 044703 (2016).

[66] B. C. Garrett, G. K. Schenter, and A. Morita, "Molecular simulations of the transport of molecules across the liquid/vapor interface of water," Chemical Reviews **106**, 1355–1374 (2006).

[67] L. Casalino, Z. Gaieb, J. A. Goldsmith, C. K. Hjorth, A. C. Dommer, A. M. Harbison, C. A. Fogarty, E. P. Barros, B. C. Taylor, J. S. McLellan, *et al.*, "Beyond shielding: the roles of glycans in the SARS-CoV-2 spike protein," ACS Central Science **6**, 1722–1734 (2020).

[68] S. Stephan, M. Dyga, H. M. Urbassek, and H. Hasse, "The influence of lubrication and the solid–fluid interaction on thermodynamic properties in a nanoscopic scratching process," Langmuir **35**, 16948–16960 (2019).

[69] S. Stephan, M. Dyga, I. A. Alhafez, J. Lenhard, H. M. Urbassek, and H. Hasse, "Reproducibility of atomistic friction computer experiments: a molecular dynamics simulation study," Molecular Simulation **47**, 1509–1521 (2021).

[70] Y. Zhang, A. Otani, and E. J. Maginn, "Reliable viscosity calculation from equilibrium molecular dynamics simulations: A time decomposition method," Journal of Chemical Theory and Computation **11**, 3537–3546 (2015).

[71] S. Stephan and H. Hasse, "Molecular interactions at vapor-liquid interfaces: Binary mixtures of simple fluids," Physical Review E **101**, 012802 (2020).

[72] S. Stephan and H. Hasse, "Interfacial properties of binary mixtures of simple fluids and their relation to the phase diagram," Physical Chemestry Chemical Physics **22**, 12544–12564 (2020).

[73] S. Stephan and H. Hasse, "Influence of dispersive long range interactions on properties of vapour-liquid interfaces of binary Lennard-Jones mixtures," Molecular Physics **118**, e1699185 (2020).

[74] S. Stephan and H. Hasse, "Enrichment at vapour-liquid interfaces of mixtures: Establishing a link between nanoscopic and macroscopic properties," International Reviews in Physical Chemistry **39**, 319–349 (2020).

[75] G. Rutkai, M. Thol, R. Span, and J. Vrabec, "How well does the Lennard-Jones potential represent the thermodynamic properties of noble gases?" Molecular Physics **115**, 1104–1121 (2017).

[76] S. Stephan, M. Horsch, J. Vrabec, and H. Hasse, "MolMod - an open access database of force fields for molecular simulations of fluids," Molecular Simulation **45**, 806–814 (2019).

[77] M. P. Allen and D. J. Tildesley, *Computer Simulation of Liquids* (Oxford University Press, Oxford, 1989).

[78] H. A. Lorentz, "Ueber die Anwendung des Satzes vom Virial in der kinetischen Theorie der Gase," Annalen Der Physik **248**, 127–136 (1881).

[79] D. Berthelot, "Sur le mélange des gaz," Comptes rendus hebdomadaires des séances de l'Académie des Sciences **126**, 1703–1706 (1898).

[80] M. Heier, S. Stephan, J. Liu, W. G. Chapman, H. Hasse, and K. Langenbach, "Equation of state for the Lennard-Jones truncated and shifted fluid with a cut-off radius of 2.5σ based on perturbation theory and its applications to interfacial thermodynamics," Molecular Physics **116**, 2083–2094 (2018).

[81] S. Stephan, M. Thol, J. Vrabec, and H. Hasse, "Thermophysical properties of the Lennard-Jones fluid: Database and data assessment," Journal of Chemical Information and Modeling **59**, 4248–4265 (2019).

[82] C. Niethammer, S. Becker, M. Bernreuther, M. Buchholz, W. Eckhardt, A. Heinecke, S. Werth, H.-J. Bungartz, C. W. Glass, H. Hasse, J. Vrabec, and M. Horsch, “ls1 mardyn: The massively parallel molecular dynamics code for large systems,” Journal of Chemical Theory Computation **10**, 4455–4464 (2014).

[83] S. Werth, M. Kohns, K. Langenbach, M. Heilig, M. Horsch, and H. Hasse, “Interfacial and bulk properties of vapor-liquid equilibria in the system toluene + hydrogen chloride + carbon dioxide by molecular simulation and density gradient theory + PC-SAFT,” Fluid Phase Equilibria **427**, 219–230 (2016).

[84] S. Stephan, J. Liu, K. Langenbach, W. G. Chapman, and H. Hasse, “Vapor-liquid interface of the Lennard-Jones truncated and shifted fluid: Comparison of molecular simulation, density gradient theory, and density functional theory,” The Journal of Physical Chemistry C **122**, 24705–24715 (2018).

[85] M. Roeselová, J. Vieceli, L. X. Dang, B. C. Garrett, and D. J. Tobias, “Hydroxyl radical at the air-water interface,” Journal of the American Chemical Society **126**, 16308–16309 (2004).

[86] J. Vieceli, M. Roeselova, N. Potter, L. X. Dang, B. C. Garrett, and D. J. Tobias, “Molecular dynamics simulations of atmospheric oxidants at the air-water interface: solvation and accommodation of OH and O_3,” The Journal of Physical Chemistry B **109**, 15876–15892 (2005).